Transmembrane proteoglycans control stretch-activated channels to set cytosolic calcium levels

Sandeep Gopal,[1,2] Pernille Søgaard,[1,2] Hinke A.B. Multhaupt,[1,2] Csilla Pataki,[1,2] Elena Okina,[1,2] Xiaojie Xian,[1,2] Mikael E. Pedersen,[2] Troy Stevens,[3,4] Oliver Griesbeck,[5] Pyong Woo Park,[6,7] Roger Pocock,[2] and John R. Couchman[1,2]

[1]Department of Biomedical Sciences and [2]Biotech Research and Innovation Center, University of Copenhagen, 2200 Copenhagen, Denmark
[3]Department of Pharmacology and [4]Department of Medicine, Center for Lung Biology, University of South Alabama, Mobile, AL 36688
[5]Max Planck Institute of Neurobiology, 82152 Martinsried, Germany
[6]Division of Newborn Medicine and [7]Division of Respiratory Diseases, Children's Hospital, Harvard Medical School, Boston, MA 02115

Transmembrane heparan sulfate proteoglycans regulate multiple aspects of cell behavior, but the molecular basis of their signaling is unresolved. The major family of transmembrane proteoglycans is the syndecans, present in virtually all nucleated cells, but with mostly unknown functions. Here, we show that syndecans regulate transient receptor potential canonical (TRPCs) channels to control cytosolic calcium equilibria and consequent cell behavior. In fibroblasts, ligand interactions with heparan sulfate of syndecan-4 recruit cytoplasmic protein kinase C to target serine714 of TRPC7 with subsequent control of the cytoskeleton and the myofibroblast phenotype. In epidermal keratinocytes a syndecan–TRPC4 complex controls adhesion, adherens junction composition, and early differentiation in vivo and in vitro. In *Caenorhabditis elegans,* the TRPC orthologues TRP-1 and -2 genetically complement the loss of syndecan by suppressing neuronal guidance and locomotory defects related to increases in neuronal calcium levels. The widespread and conserved syndecan–TRPC axis therefore fine tunes cytoskeletal organization and cell behavior.

Introduction

Cell surface heparan sulfate is essential in bilaterian development and has regulatory roles in tissue repair and inflammation as well as the pathophysiology of tumor progression, vascular disease, and inflammation (Li et al., 2002; Bishop et al., 2007; Stanford et al., 2009; Pap and Bertrand, 2013; Ramani et al., 2013; Barbouri et al., 2014). The two major classes of heparan sulfate proteoglycan are the glycosylphosphatidylinositol-anchored glypicans and transmembrane syndecans. Both have a long evolutionary history, being present in invertebrates where their roles in the developing nervous system have been demonstrated (Rhiner et al., 2005). However, signaling roles for invertebrate syndecan core protein are unknown. Moreover, for the most part, the mechanism by which protein ligands for cell surface polysaccharides such as heparan sulfate exert their effects in vertebrate systems is also poorly known. The cytoplasmic domains of syndecans can be divided into three small regions, two of which are highly conserved (C1 and C2) and are membrane proximal and membrane distal. Between them is a variable region that is specific to each syndecan, but nevertheless conserved across species (Woods and Couchman, 1998). All four mammalian syndecans can link to the actin cytoskeleton (Kinnunen et al., 1998; Greene et al., 2003; Chen and Williams, 2013), which relates to trafficking and recycling of syndecans and their associated receptors such as integrins (Bass et al., 2011; Morgan et al., 2013; Chen and Williams, 2013) as well as exosome formation (Baietti et al., 2012). In addition, our previous work (Couchman, 2010) and that of others (Morgan et al., 2007) demonstrated that one vertebrate proteoglycan, syndecan-4, is a key contributor to cell–extracellular matrix junction formation, and thereby cell adhesion and migration. Mesenchymal cells lacking this receptor do not acquire a myofibroblastic phenotype characteristic of their wild-type (wt) counterparts (Okina et al., 2012). The variable region of syndecan-4, interacting with both cytoskeleton and signaling molecules (PKCα), is key to junction assembly (Oh et al., 1997; Horowitz and Simons, 1998; Mostafavi-Pour et al., 2003). Consistent with these observations, syndecans have

Correspondence to John R. Couchman: john.couchman@bric.ku.dk

S. Gopal and R. Pocock's present address is Monash Biomedicine Discovery Institute and Dept. of Anatomy and Developmental Biology, Monash University, Melbourne, Victoria 3800, Australia.

P. Søgaard's present address is Kennedy Institute of Rheumatology, University of Oxford, Oxford OX3 7FY, UK.

C. Pataki's present address is Dept. Cell Biology, Faculty of Science, Charles University in Prague, 128 43 Prague 2, Czech Republic.

E. Okina's present address is Program in Cardiovascular and Metabolic Disorders, Duke–National University of Singapore Graduate Medical School, Singapore, Singapore.

Abbreviations used in this paper: αSMA, α-smooth muscle actin; ANOVA, analysis of variance; FRET, Förster resonance energy transfer; KO, knockout; MEF, mouse embryonic fibroblast; TRP, transient receptor potential; TRPC, TRP canonical; wt, wild type.

The Rockefeller University Press $30.00
J. Cell Biol. Vol. 210 No. 7 1199–1211
www.jcb.org/cgi/doi/10.1083/jcb.201501060

been assigned roles in wound repair in vivo (Echtermeyer et al., 2001; Stepp et al., 2002). However, although ablation of genes involved in heparan sulfate synthesis has severe consequences, the same is not true of syndecan core protein knockouts (KOs; Echtermeyer et al., 2001; Stepp et al., 2002; Bishop et al., 2007). This has led to the notion that there is redundancy across the vertebrate syndecan core proteins, but no molecular basis for this hypothesis has been forthcoming until now. Here we propose that invertebrate and vertebrate syndecans regulate calcium channels of the transient receptor potential (TRP) type and that this is one mechanistic explanation for their roles in adhesion and junction assembly.

Results

The myofibroblastic phenotype is regulated by syndecan-4 control of cytosolic calcium

Our comparative microarray analysis of wt (wt) and syndecan-4 null (s4ko) fibroblasts has shown that despite actin cytoskeletal differences between these two cell types, there were no key differences in transcriptomic analysis of cytoskeletal or receptor protein expression (Okina et al., 2012). However, alterations in some calcium-regulated pathways (calcineurin–NFAT–RCAN-2) were observed that were supported by immunochemical analysis of the cells (Fig. S1) and previous work on cardiac hypertrophy in s4ko animals (Martínez-Martínez et al., 2009; Echtermeyer et al., 2011; Finsen et al., 2011). To explore this further, the Twitch-1 ratiometric sensor (Thestrup et al., 2014) was used to measure the calcium status in s4ko and matching wt fibroblasts. This revealed consistently elevated cytosolic calcium levels in s4ko cells (Fig. 1, A and B; Fig. S1; and Videos 1, 2, and 3). To confirm the specificity of this observation, syndecan-4 was reexpressed in s4ko cells, whereupon calcium levels decreased to wt levels (Fig. 1, A and B; and Videos 1, 2, and 3). In addition, siRNA depletion of syndecan-4 from primary rat embryo fibroblasts was followed by calcium elevation (Fig. 1, C and D). Cytosolic calcium levels in fibroblasts are, therefore, controlled by the syndecan. Syndecan-4 consists of an ectodomain bearing three heparan sulfate chains, a single transmembrane domain, and a short cytoplasmic domain that is divided into three motifs, the central one of which binds and activates PKCα (Oh et al., 1997; Couchman, 2010). To ascertain how syndecan-4 functions in calcium metabolism, two mutant forms were expressed in s4ko fibroblasts. The first lacked all heparan sulfate chains by replacement of the three relevant serine residues by alanine and the second was C-terminally truncated in the variable region to prevent PKCα binding and activation (Gopal et al., 2010). Neither mutant form of syndecan-4, when expressed in s4ko cells, could reset calcium levels to those of wt cells (Fig. 1, E and F). However, a shorter truncation to remove the C2 region alone was at least partly functional in terms of reducing calcium levels, suggesting that PDZ protein binding to syndecan-4 may not be the major determinant of calcium regulation (Fig. 1 G).

In previous experiments with fibronectin as a model extracellular matrix glycoprotein, we showed that focal adhesion formation was promoted by a combination of integrin and syndecan-4 binding to distinct domains (Woods et al., 1986). The major RGD-containing $FnIII_{10}$ repeat is known for its integrin-binding capacity (Fig. 1 H; Morgan et al., 2007), whereas the HepII domain ($FnIII_{12–14}$) interacts with the heparan sulfate chains of syndecan-4 with downstream PKCα activation (Fig. 1 H). Both interactions are required for focal adhesion assembly (Dovas et al., 2006; Morgan et al., 2007; Couchman, 2010). These experiments were revisited to assess cytosolic calcium levels. wt primary fibroblasts spread on the $FnIII_{6–10}$ fibronectin polypeptide had higher calcium levels than those seeded on whole fibronectin (Fig. 1 I). Triggering of syndecan-4 by addition of $FNIII_{12–15}$ domain to cells spread on the $FNIII_{6–10}$ domain led to a rapid decrease in calcium to levels equivalent to cells on whole fibronectin (Fig. 1 I and Video 4). This effect was not seen in s4ko cells, where calcium levels remained unchanged or where PKC was inhibited in wt cells (Figs. 1, J and K). In total, the data suggest that syndecan-4, when binding ligands through its heparan sulfate chains, regulates cytosolic calcium in a PKC-dependent manner.

We hypothesized that syndecan-4 controls one or more calcium channels. Transcriptomic analysis revealed over 20 channel types in both wt and s4ko cells (Fig. S1). A combination of pharmacological (Fig. S2) and siRNA depletion experiments (Figs. 2 and S2) identified a single channel, TRPC7, involved in syndecan-4 function. This channel was uniquely present in focal adhesions (Fig. 2 A), consistent with syndecan-4's role, in a complex with syndecan-4 and α-actinin (Fig. 2 B). The codistribution with α-actinin was confirmed by confocal microscopy coupled with line scanning (Fig. 2 C), consistent with a previous study of TRPC6 association with this cytoskeletal component (Goel et al., 2005). Crucially, depletion of TRPC7, but not TRPC1, in s4ko cells led to decreased calcium equivalent to that of wt cells (Fig. 2 D) and formation of stress fibers and focal adhesions (Fig. 2, E and F). These phenotypic changes could not be reproduced by depletion of other TRP channels (Fig. S2 B). Moreover, Western blotting demonstrated that TRPC7 siRNA had no effect on protein levels of the related TRPC1, 3, or 6 channels (Fig. S2). Depletion of TRPC7 in wt fibroblasts had no discernible impact on the cytoskeleton or calcium (Fig. S2), indicating that the presence of syndecan-4 controls TRPC7 functional status.

Two established molecular characteristics of the myofibroblast are the presence of α-smooth muscle actin (αSMA) in stress fibers and OB-cadherin (cadherin 11) in adherens junctions (Hinz et al., 2004). Although both these features are present in our wt fibroblasts, s4ko cells lack of αSMA in microfilament bundles and use N-cadherin in adherens junctions (Figs. 2 and 3, A and B). The s4ko cells expressed OB-cadherin, but neither inserted it into adherens junctions nor transported it to the cell surface (Fig. 3 C). Reexpression of wt syndecan-4 in s4ko cells restored OB-cadherin to adherens junctions (Fig. S2 G). However, expression of the two mutant forms of syndecan 4, either lacking heparan sulfate chains or with a truncated cytoplasmic domain, failed to do so (Fig. S2 G). Depletion of TRPC7 in the s4ko cells, on the other hand, led to the acquisition of wt cytoskeleton and junctions, including replacement of N-cadherin with OB-cadherin at adherens junctions (Figs. 3, D and E). Therefore, it appears that syndecan-4 regulation of TRPC7 is required for the maintenance of the myofibroblastic phenotype.

Syndecan-1 is not a major determinant of fibroblast adhesion phenotype

The primary fibroblasts used here possess syndecan-1 in addition to syndecan-4 (Fig. S3 A). To assess whether syndecan-1 had a contributory role to calcium levels and the actin cytoskel-

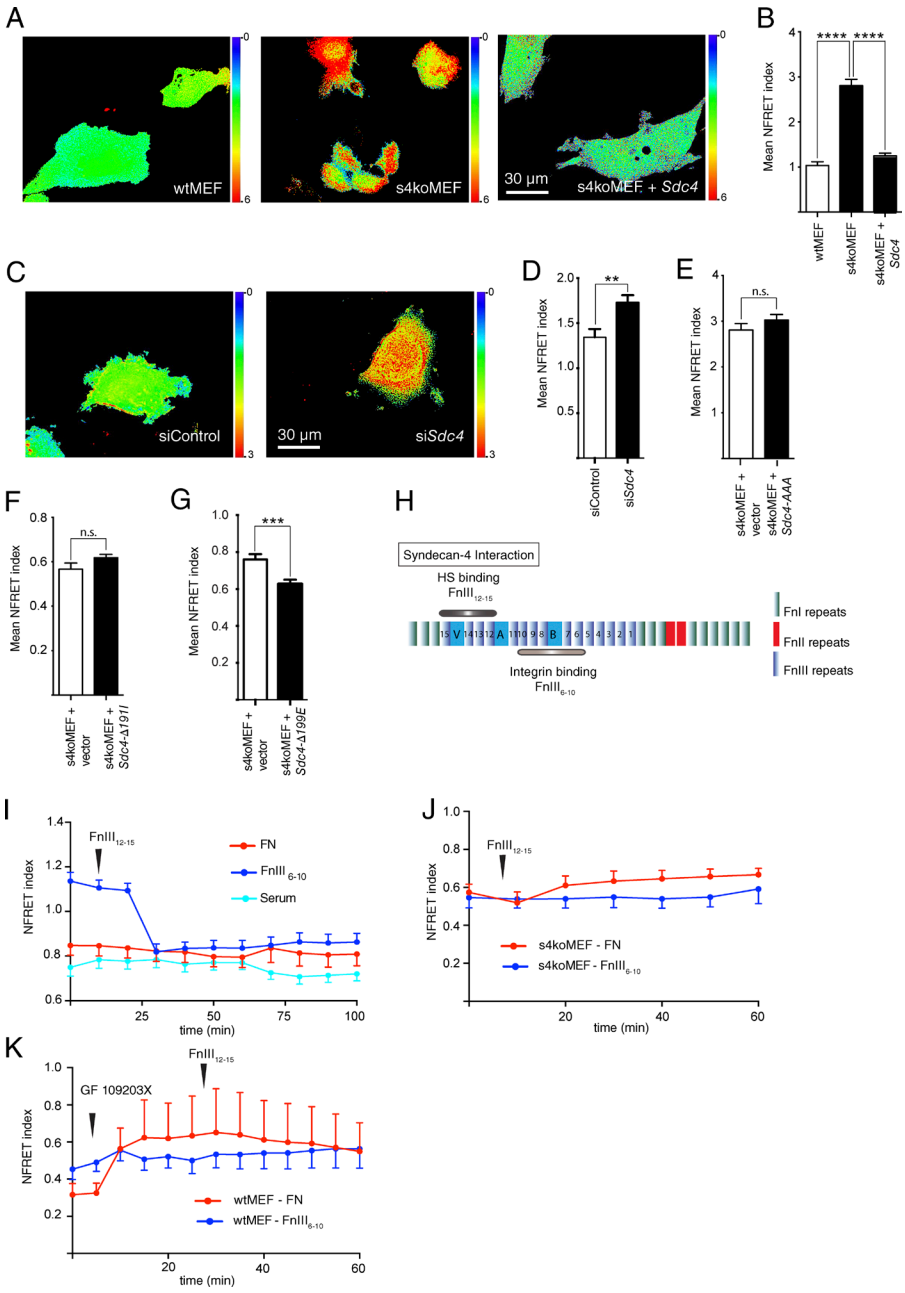

Figure 1. **Calcium metabolism is altered in the absence of syndecan-4.** (A and B) FRET analysis using *Twitch-1* reveals elevated calcium levels in s4ko MEF compared with matching wt counterparts. Re-expression of *Sdc4* in s4ko cells reduces calcium to wt levels. n = 115 for wtMEF; n = 90 for s4ko MEF; n = 120 for s4ko + wt MEF. (C and D) Reduction of syndecan-4 in rat embryonic fibroblasts leads to elevated cytosolic calcium. n = 63 in D. (E–G) Ectopic expression of *Sdc4* mutant forms lacking heparan sulfate chains (*Sdc4-AAA*) or a truncated cytoplasmic domain (*Sdc-Δ191I*) do not restore calcium to wt levels. However, expression of *Sdc4* mutant lacking the C2 domain (*Sdc-Δ199E*) resulted in reduced calcium levels. n = 55–120 per condition. (H) Diagram of fibronectin domains and interactions of syndecan-4 leading to PKCα activation. (I–K) wt MEFs plated on $FnIII_{6–10}$ protein have elevated cytosolic calcium levels compared with those plated on full-length fibronectin or serum-coated surfaces, but undergo reduction in response to $FnIII_{12–15}$ protein addition (I). (J) s4ko MEF on $FnIII_{6–10}$ protein or full-length fibronectin possessed similar, high calcium levels that are unchanged by addition of $FnIII_{12–15}$ protein. (K) Treating wt MEFs plated on $FnIII_{6–10}$ with GF109203x did not increase calcium levels but in this case the addition of $FnIII_{12–15}$ failed to reduce the cytosolic calcium level. Additionally, wt MEF on whole fibronectin elevate calcium in response to PKC inhibition that is also unchanged after $FnIII_{12–15}$ addition. See also Videos 1, 2, 3, and 4. Data are the mean ± SEM. ****, $P < 0.0001$; ***, $P < 0.001$; **, $P < 0.01$; unpaired t test.

eton, its levels were reduced by siRNA (Fig. S3 A). This had no impact on cytosolic calcium, αSMA organization, focal adhesion assembly, TRPC7 presence in focal adhesions, or cadherin utilization in adherens junctions (Figs. 2 A and S3, B and C).

In a further series of experiments, primary dermal fibroblasts were derived from wt, s4ko, s1ko, and double s1s4ko mice. Calcium levels and microfilament bundle formation and TRPC7 localization were quantified (Fig. S3, D–F). Calcium levels were increased with loss of syndecan-1, but not to the same extent as loss of syndecan-4. Moreover, there was no additive effect on calcium levels by loss of both syndecans. Similarly, absence of syndecan-1 had no significant effect on microfilament bundle organization or TRPC7 localization (Fig. S3, E and F). Therefore, it appeared that syndecan-1 can contribute to calcium status but without substantial impact on adhesion morphology of primary fibroblasts. However, these experiments further validated the distinctions between wt and s4ko fibroblasts in terms of calcium and adhesive phenotype because the cells were derived from mice of completely distinct genetic background from those shown in Figs. 1, 2, and 3.

TRPC7 is regulated at serine714

In common with all TRP canonical (TRPC) channels, a key TRP motif is located proximal to the most C-terminal transmembrane domain, known to be important in channel gating (Venkatachalam and Montell, 2007). An adjacent serine residue is subject to PKC phosphorylation in TRPC3, a close homologue of TRPC7 (Fig. 3 F; Trebak et al., 2005), which leads to channel closure. Therefore, we constructed two mutants of TRPC7 where serine714 was changed to alanine or phosphomimetic glutamate. These were expressed in wt fibroblasts along with the wt TRPC7 cDNA as a control. Expression of the ser-714ala mutant channel led to elevated calcium and loss of focal adhesions, an effect not replicated by overexpression of the

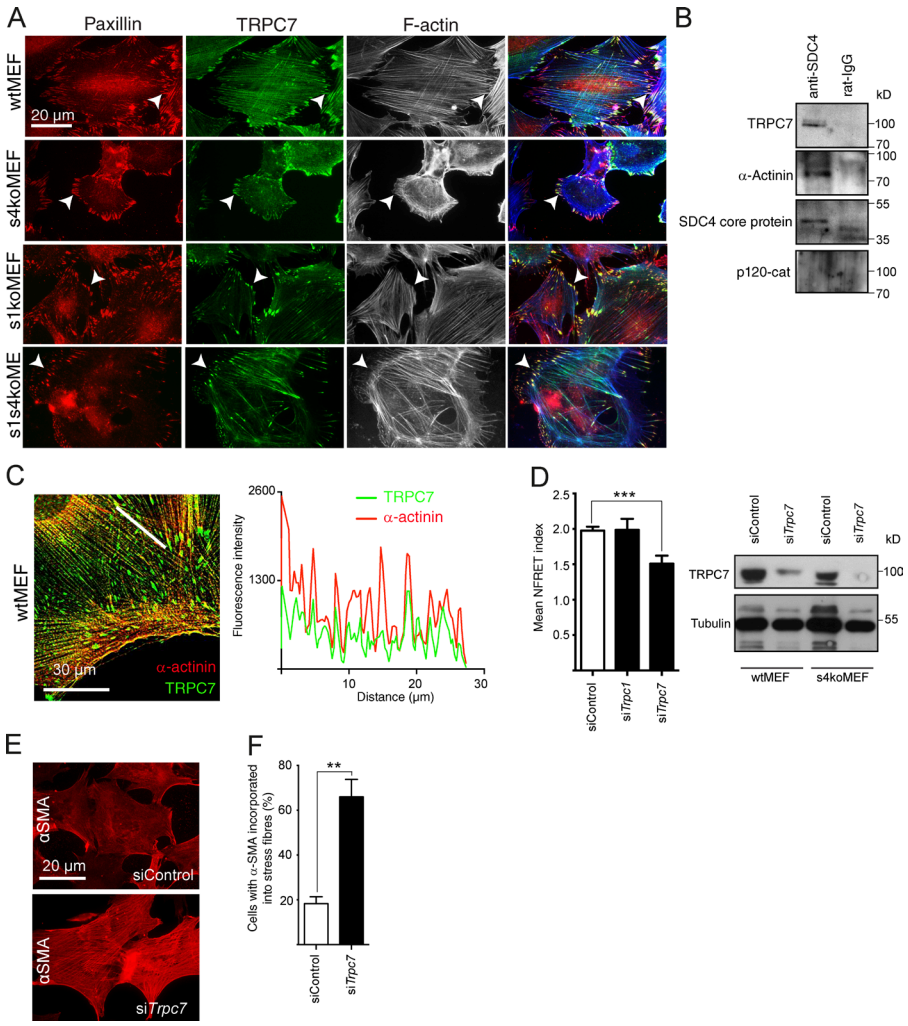

Figure 2. **TRPC7 is associated with syndecan-4 and focal adhesions.** (A) Immunostaining of wt, s4ko, s1ko, and s1S4 double KO MEFs shows colocalization of TRPC7 with paxillin at focal adhesions (arrowheads). Fewer focal adhesions and stress fibers were noted in s4ko and s1s4ko MEFs. (B and C) Syndecan-4 clustering on wt MEF cell surfaces with core protein–directed antibody followed by cell lysis and Western blotting shows copurifying TRPC7 and α-actinin, a known binding partner of syndecan-4, but not p120 catenin. Confocal microscopy with line scanning of wt MEF cells shows coalignment of TRPC7 and α-actinin. The data shown are from a single representative cell out of three experiments. (D) Silencing TRPC7, but not TRPC1, gene expression results in a reduction of calcium in s4ko MEFs. $n = 20$ for control and TRPC1 siRNA and $n = 72$ for TRPC7 siRNA. (E and F) Knockdown of TRPC7 in s4ko MEFs increases stress fibers containing αSMA. $n > 100$ cells per condition in F. Data are mean ± SEM. ***, $P < 0.001$; **, $P < 0.01$; unpaired *t* test.

ser714glu mutant (Fig. 3 G). The same series of TRPC7 constructs were additionally expressed in s4ko fibroblasts. Calcium levels were unchanged in response to wt TRPC7 expression, but increased further in response to ser714ala mutant. In contrast, calcium levels decreased where the ser714glu mutant protein was expressed (Fig. 3 H). Correspondingly, where calcium levels decreased, with ser714glu expression, the proportion of cells with organized αSMA-containing stress fibers and OB-cadherin utilization at adherens junctions increased. Where calcium levels were unchanged or were further elevated, no change in the cytoskeleton or adherens junctions was noted compared with control s4ko cells (Fig. 3 H).

In total, it appears that the syndecan-4–PKCα axis controls TRPC7 channel through phosphorylation of ser714, and in the absence of the proteoglycan, the channel has a higher probability of being open, leading to elevated calcium levels.

Epithelial syndecans control cytosolic calcium with impact on cell adhesion

To determine whether the regulation of a TRPC channel is unique to syndecan-4, a mammalian epithelial system was investigated. Because syndecan-1 is known to be important in epidermal repair (Stepp et al., 2002), we investigated this tissue through in vitro and in vivo experiments. HaCaT epithelial cells proliferate in low extracellular calcium, but differentiate with formation of cadherin-containing adherens junctions when levels are raised. They express mostly syndecan-1, but also some syndecan-4. No syndecan-2 or -3 was detectable (Fig. 4 A), even where syndecan-1 and -4 were suppressed by siRNA treatment (Fig. S4). Depletion of syndecans by siRNA caused changes in cytosolic calcium levels, consistent with regulation by TRPC channels (Fig. 4 B). However, it was notable that depletion of both syndecans was required before this change was observed. Consequently, there is redundancy between the two syndecans; when only one was reduced by siRNA, there was no impact on cytosolic calcium (Fig. 4 B). Double siRNA treatment to reduce syndecan-1 and -4 levels had no influence on protein levels of any TRPC channel investigated (TRPC1, 3, 4, and 6; unpublished data). In epithelial cells, an association of both syndecans with TRPC4 was noted (Fig. 4 C), and consistent with this, depletion of TRPC4, but not other TRPCs (Fig. S4), had the same effect on calcium as syndecan-1 and -4 siRNA treatment (Fig. 4 D). Along with altered calcium levels, both syndecan and TRPC4 depletion led to reduced expression of the differentiation markers keratin 1 and involucrin but not that of the basal keratin 5 (Fig. 4 E), suggesting a hindrance in early differentiation. Consistent with roles in cell adhesion and junction formation, depletion of both syndecans or TRPC4 resulted in a marked expression of P-cadherin (cadherin 3) in adherens junctions (Fig. 4, F and G), along with E-cadherin (not depicted). Deletion of a single syndecan was insufficient to promote P-cadherin ex-

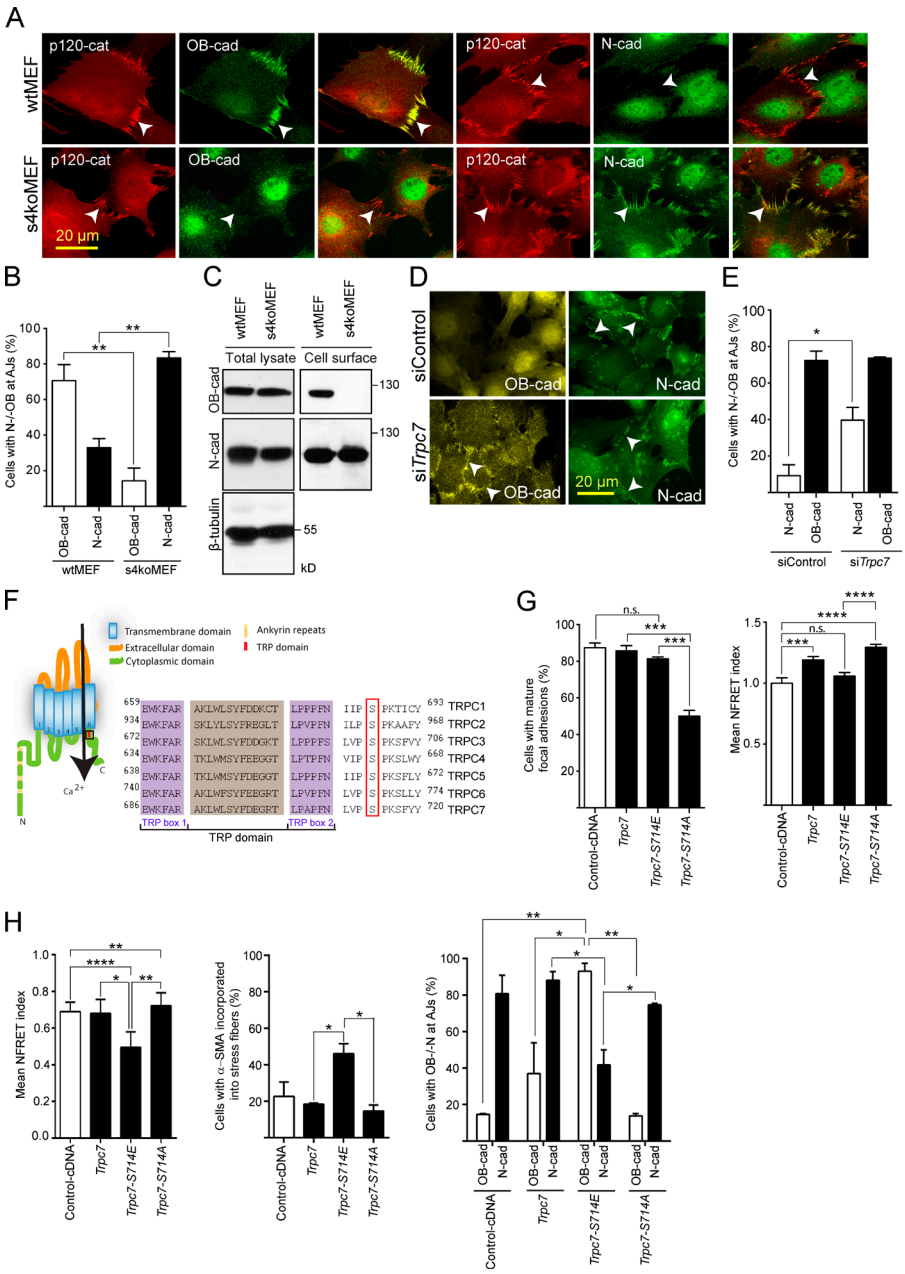

Figure 3. **TRPC7 is regulated by PKC-mediated phosphorylation of serine714.** (A and B) wt and s4ko cells have different adherens junction (AJ) composition, the former using OB-cadherin, whereas s4ko MEFs use to N-cadherin (arrowheads). Quantitation of cadherin colocalization with the junction maker p120 catenin is shown in B. Triplicate experiments were performed with $n > 100$ cells of both types. (C) Cell surface biotinylation shows that N-cadherin was expressed on the surface of both cell types whereas OB-cadherin was expressed only on the surface of wt MEFs. (D and E) Silencing of TRPC7 expression in s4ko MEF led to the restoration of OB-cadherin to adherens junctions (arrowheads), thereby resembling wt MEFs even in the continued absence of syndecan-4. Triplicate experiments were performed with $n > 50$ cells each. (F) Structure of TRPC channels. The semi-conserved TRP domain following the sixth transmembrane domain is boxed and its sequence is shown to the right. A conserved serine residue immediately C-terminal of the TRP domain is marked with a red box. (G and H) wt (G) and s4ko (H) MEFs were transfected with cDNAs encoding wt (*Trpc7*), phosphomimetic (*Trpc7-S714E*), and phospho-resistant (*Trpc7-S714A*) mutant forms of TRPC7. 50% of the wt cells transfected with *Trpc7-S714A* failed to form mature focal adhesions and possessed higher cytosolic calcium levels than control cells. *Trpc7-S714E* expressing cells show no significant elevation in cytosolic calcium. (H) The same constructs transfected into s4ko cells. Calcium was only reduced in cells expressing *Trpc7-S714E*, with corresponding increase in stress fibers and OB-cadherin usage in adherens junctions. Triplicate experiments were performed. (G) n = 30 cells for each condition (left); n = 45–101 cells per condition (right). (H) n = 32–65 cells per condition (left), >200 cells per condition (middle); and n = 30–100 cells per condition in duplicate (right). Data are the mean ± SEM. ****, $P < 0.0001$; ***, $P < 0.001$; **, $P < 0.01$; *, $P < 0.05$; unpaired *t* test.

pression in junctions, again suggesting redundancy between syndecan-1 and -4 (Fig. S4). Therefore, as with fibroblasts, junction formation involving the actin cytoskeleton is regulated by syndecans and TRPCs.

To confirm these results, we examined epidermis from mice harboring a single syndecan-1 or -4 KO or from the double syndecan KO mouse. Consistent with the in vitro data, strong expression of P-cadherin in the basal layers of the epidermis was observed in the double syndecan KO mouse (Fig. 4 H), but not in either of the single KOs (Fig. S4 C) or wt animals (Fig. 4 H). Moreover, disturbances in the organization of the lower epidermal layers were noted in the double syndecan null, whereby suprabasal cells, marked by keratin 10, retained cytoplasmic extensions between basal cells to contact the basement membrane (dermal–epidermal junction; Fig. 4 I). These were not visible in epidermis from single syndecan null mice (Fig. S4 D). The disturbed epidermal organization was quantified by electron microscopic morphometry (Figs. 4 J and S4 F), yielding identical results to epidermis derived from the TRPC4 null rat skin. Therefore, adhesion alterations resulted from disturbance of the syndecan–TRPC axis in epithelia, both in vitro and in vivo. It should be noted, however, that late stages of differentiation including the morphology of the granular layer and stratum corneum appeared normal in both the syndecan-1/4 double null skin and that of TRPC4 null skin. The surface appearance of the skin and hair follicles was normal, consistent with prior data showing that syndecans are present predominantly in the lower layers of the epidermis and that TRPC4 functions in early differentiation events (Beck et al., 2008; Leuner et al., 2011).

In summary, syndecan heparan sulfate proteoglycans set cytosolic calcium as a mechanism to control cell adhesion, actin cytoskeleton, and junction formation. This is achieved through the control of TRPC channels.

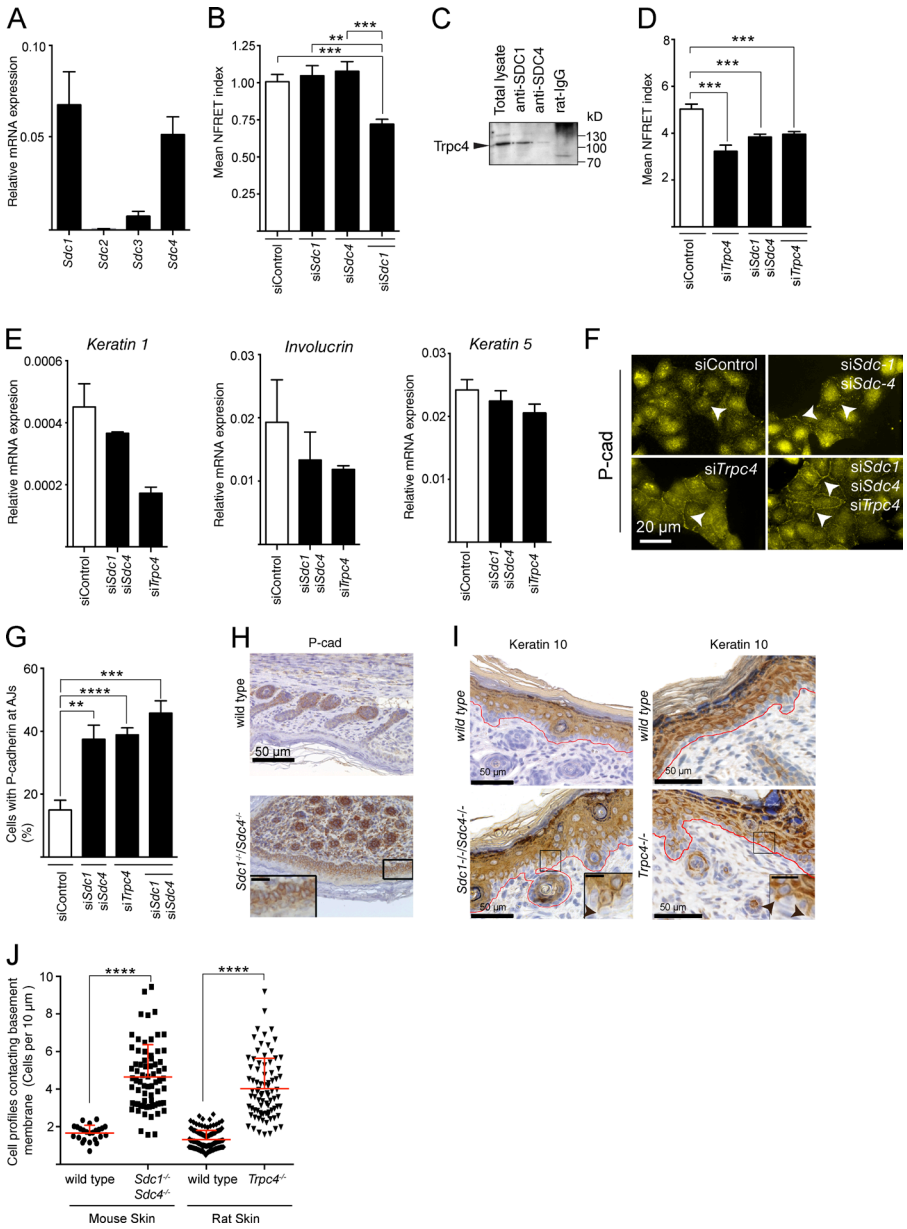

Figure 4. **Syndecan regulation of calcium and cell adhesion through TRPC4 in epithelial cells.** (A) Syndecan expression in HaCaT cells was analyzed by quantitative RT-PCR. Syndecan-1 and -4 were expressed highly in contrast to syndecan-2 and -3. (B) Single knockdown of syndecan-1 or -4 in HaCaT epidermal cells does not affect cytosolic calcium levels, whereas reduction of both proteoglycans yields reduced cytosolic calcium. n = 26–56. (C) TRPC4 associates with syndecan-1 and -4. Specific syndecan antibodies were used to cluster and precipitate complexes that were probed for TRPC4. Normal rat IgG was used as a control. (D) Silencing TRPC4 in HaCat cells reduces cytosolic calcium similar to that of double syndecan-1/4 knockdown. Combining siRNA for the syndecans and TRPC4 together does not further reduce cytosolic calcium. n > 40 cells in each case. (E) Differentiation markers keratin 1 and involucrin, but not basal keratin 5, mRNA levels were decreased on reduction of syndecan-1 and -4 or TRPC4 (n = 3). (F and G) P-cadherin immunocytochemistry in HaCat cells silenced for syndecan-1 and -4 showed an increase at adherens junctions (arrowheads) after 4 h of culture in high calcium medium to stimulate differentiation. Similar effects are seen in cells silenced for TRPC4 expression or TRPC4 silenced in a syndecan null background. Data are shown from five replicates. (H) wt newborn murine skin contains no discernible P-cadherin in interfollicular epidermis, but it is strongly expressed in the basal and spinous layers of the syndecan-1/4 double KO tissue. (I) Keratin 10 is strictly suprabasal in wt mouse (left) and rat skin (right), but keratin 10–positive cytoplasmic extensions to the basement membrane (marked in red) are present in the syndecan null and TRPC4 null epidermis (arrowheads). Insets in H and I show higher magnification images of boxed areas. Bars, 10 µm. (J) Electron micrographs of skin samples from two different tissue blocks from neonate wt mouse and rat skin, s1s4 double KO mouse, and TRPC4 KO rat skin were analyzed (examples shown in Fig. S3 E). Total discrete cell profiles in contact with the dermal–epidermal junction were quantitated. A total of 24 frames (86 cells) for mouse wt, 70 frames (454 cells) for s1s4 KO mouse, 127 frames (148 cells) for wt rat, and 82 frames (208 cells) for TRPC4 KO rat were quantitated. Statistical analysis was performed and group differences were determined using unpaired t test. ****, $P < 0.0001$ for both sets of null animals versus their respective wt controls. See also Fig. S3. Data are the mean ± SEM. ****, $P < 0.0001$; ***, $P < 0.001$; **, $P < 0.01$; unpaired t test.

TRP channels are regulated by invertebrate syndecan

From the preceding data, mammalian syndecans have a major role in calcium channel regulation. If this property is fundamental to all syndecans, it should also be conserved. To test this hypothesis, studies in *Caenorhabditis elegans*, which only expresses one syndecan, were performed. In embryos, the PVQ and HSN neurons undergo aberrant guidance in the absence of the single syndecan (Fig. 5 A; Rhiner et al., 2005). The nematode has three TRP channels that are orthologues of the TRPC channels of mammals. Of these, TRP-1 and TRP-2 are widely expressed, whereas TRP-3 is restricted to sperm cells (Xiao and Xu, 2009). We therefore analyzed the effect of TRP-1/2 loss in a syndecan mutant strain using three assays. First, it was assessed whether the absence of TRP-1 and -2 could ameliorate the effects of syndecan absence on guidance of the HSN and PVQ neurons (Rhiner et al., 2005). The absence of the two TRP channels had no impact on the guidance of these neurons. In contrast, guidance defects of syndecan mutant animals were partially suppressed by loss of TRP-1 and -2 (Fig. 5, B and C). Therefore, the absence of TRP-1 and -2 partially complemented the absence of syndecan.

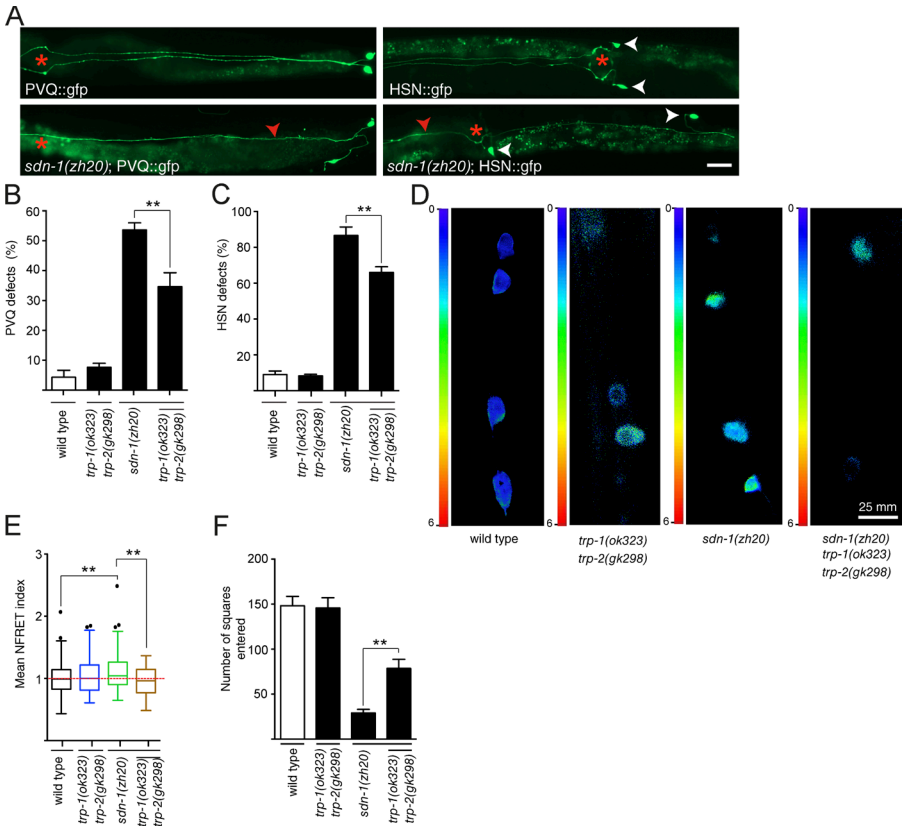

Figure 5. ***sdn-1* mutant neurodevelopmental and behavioral defects are dependent on TRPC channels in *C. elegans***. (A) In wt animals, PVQ neurons extend anteriorly-directed axons from the tail. The axons navigate the left and right ventral nerve cord fascicles where axons are separated by the hypodermal ridge. In *sdn-1(zh20)* mutant animals, PVQ axons are misguided, with crossover to the contralateral side of the ventral nerve cord (red arrowhead). In wt animals, HSN cell bodies migrate to a position just posterior to the vulva and extend axons in a highly stereotypical manner. Their axons extend ventrally, and then around the vulva before entering the ventral nerve cord where each axon is separated by the hypodermal ridge. In *sdn-1(zh20)* mutant animals, HSN cell bodies do not migrate to their correct position and their axons are misguided. Cell bodies are shown with white arrowheads and misguided axons by red arrowheads. Vulval position is marked with red asterisks. Ventral view, anterior to the left in all cases. Bar, 20 µm. (B and C) Scoring of PVQ and HSN developmental defects, respectively. $n > 50$ in each case. (D and E) Calcium imaging by FRET microscopy of ventral ganglia from live immobilized animals expressing the sensor cameleon YC3.60. $n = 48–123$ per strain. (F) Scoring of exploratory behavior; $n > 15$ for each strain. Data are the means ± SEM. Statistical significance was assessed by ANOVA followed by Newman-Keuls multiple comparison test. **, $P < 0.01$ versus *sdn-1(zh20)* mutant. Data in E were analyzed by ANOVA ($P = 0.001$) followed by pairwise *t* tests with Holm correction of p-values (wt vs. sdc null, $P < 0.01$; sdc null vs. sdc+TRP1/2 null, $P < 0.005$).

Second, the same strains used above were crossed into a strain expressing a cameleon ratiometric calcium sensor in all neurons (Smith et al., 2013). Imaging by Förster resonance energy transfer (FRET) microscopy allowed calcium levels to be measured in syndecan-containing ventral motorneurons of live but immobilized animals (Fig. 5 D). Three major conclusions could be drawn from the calcium imaging. First, in the absence of syndecan, calcium levels in the ganglia were significantly elevated over those of wt animals. Second, depletion of the two TRP channels alone had no impact on cytoplasmic calcium levels. Third, the absence of TRP-1 and -2 reduced the motorneuron calcium levels in syndecan mutant animals to a level not significantly different from wt (Fig. 5 E).

In a third test, worm locomotory behavior was quantitated. Compared with wt animals, deletion of TRP-1 and -2 had no measurable impact on locomotion. However, syndecan null animals were severely compromised in their movements (Fig. 5 F). In contrast, triple mutant animals lacking syndecan and TRP-1 and -2 were significantly more motile than the syndecan mutant animals (Fig. 5 F), suggesting again that syndecan regulates the two TRP channels.

Discussion

The cumulative data suggest that a fundamental property of all syndecans is to control TRP channels. The consequences of this regulation are seen in terms of actin cytoskeleton, cell adhesion, junctions, and migration. No TRPC protein has been noted as a focal adhesion component previously, and TRPC7 deserves further attention in this regard. However, the data suggest that TRPC7 does not require syndecan-4 or -1 for focal adhesion localization, but syndecans can regulate their function. Elevated calcium in fibroblasts may impact the phosphorylation status of focal adhesion kinase and thereby focal adhesion turnover, consistent with the molecular and cytoskeletal phenotype of s4ko cells (Giannone et al., 2004). TRPC7 is therefore identified as a potentially critical regulator of myofibroblast phenotype, with implications for wound repair, fibrosis, and the tumor stroma (Rybinski et al., 2014). Because adherens junctions and focal adhesions are sites of mechanotransduction (Hayakawa et al., 2008; Smutny and Yap, 2010; Prager-Khoutorsky et al., 2011), the regulation of stretch-activated channels in their vicinity is entirely consistent with localized actin dynamics (Ambudkar et al., 2006; Hayakawa et al., 2008).

In epithelial cells, the data provide evidence of redundancy across syndecans. Deletion of both syndecan-1 and -4 was required before a clear phenotype was observed in terms of cell adhesion. The aberrant expression of P-cadherin in the interfollicular epidermis of syndecan null mice recalls two human skin diseases characterized by abnormal calcium metabolism, Hailey-Hailey and Darier's diseases (Hakuno et al., 2001). In the latter case, mutations in the SERCA channel protein are accompanied by altered TRPC expression and cytosolic calcium homeostasis (Pani et al., 2006). In addition, psoriatic epidermis has reduced TRPC protein expression, altered calcium homeostasis, and P-cadherin expression throughout the viable strata (Zhou et al., 2003; Leuner et al., 2011). As here, specific cad-

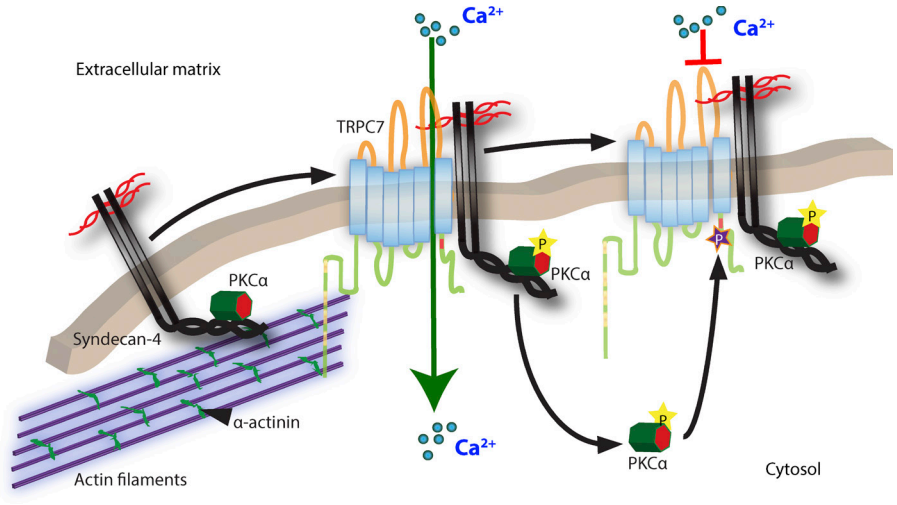

Figure 6. **Summary diagram.** Syndecan proteoglycans regulate cytoskeleton and cell behavior through their control of TRPCs. Syndecans and TRPC channels can both interact with the actin cytoskeleton. Signaling in response to heparan sulfate–binding ligands by syndecan-4 involves PKCα activation and phosphorylation of a key TRPC serine residue that controls channel opening.

herin insertion into adherens junctions appears to be linked to cytoplasmic calcium levels.

The data also provide the first evidence of a signaling role for syndecan core protein in *C. elegans*, along with evidence of conservation of function through evolution. Restoration to wt in terms of neuronal guidance or locomotory behavior was incomplete in the syndecan–TRP-1 and -2 triple mutants, but could be anticipated. In the absence of syndecan, important heparan sulfate moieties are missing from the pericellular environment, which remains the case where TRP channels are also deleted. Consistent with this, syndecan in *C. elegans* has been suggested to have noncell autonomous roles in netrin signaling (Schwabiuk et al., 2009). Several groups have shown a key role for heparan sulfate in neuronal guidance, including that of the HSN neurons (Bülow and Hobert, 2004; Kinnunen et al., 2005; Rhiner et al., 2005; Pedersen et al., 2013; Tecle et al., 2013). In total, these genetic experiments in *C. elegans* support the hypothesis that syndecan regulates the TRP-1/2 channels. This study provides the first mechanistic insight into the syndecan core protein function in the nematode and, additionally, shows that syndecan regulation of TRPC-type channels is a conserved feature of invertebrates and vertebrates. It is remarkable that this property of syndecan extends from the TRPC channels in mammals to their precise orthologues in *C. elegans*, TRP-1 and -2.

It will now be interesting to determine to what extent the many potential functions of syndecans described over the past 25 yr are partially or wholly explicable in terms of calcium regulation. Certainly the s4ko phenotype in fibroblasts appears to be solely a result of a dysregulated TRPC channel (Figs. 1, 2, 3, 6, S2, and S3). Many syndecan functions relate to the binding of growth factors, morphogens, cytokines, and chemokines through their heparan sulfate moieties, synergistically combining with high affinity receptors to effect intracellular signaling. In this context, hepatocyte growth factor/receptor-mediated cell scattering has been shown to depend on TRPC6 (Langford et al., 2012), whereas TRPC1-mediated calcium influx is required for fibroblast growth factor-2–mediated Madin-Darby canine kidney cell chemotaxis (Fabian et al., 2011). TRPC3 channels are necessary for brain-derived neurotrophic factor induction of dendritic spine formation (Amaral and Pozzo-Miller, 2007), a process also supported by syndecan-2 (Ethell et al., 2001). Last, transforming growth factor-β–promoted myofibroblast differentiation is reported to be TRPC6 dependent (Davis et al., 2012). Because these growth factors have known and essential heparan sulfate–binding properties, a convergence of syndecans on calcium regulation may apply to these and many other cases.

In conclusion, genetic analysis coupled with molecular and cellular experiments show that regulation of TRPC channels resulting in the tuning of cytosolic calcium levels is a common function of both vertebrate and invertebrate syndecans.

Materials and methods

Cell culture, plasmids, and transfection

Syndecan-4 null and matching wt murine embryonic fibroblasts (Okina et al., 2012) were grown and maintained in αMEM (Lonza) supplemented with 10% vol/vol FCS (HyClone; Thermo Fisher Scientific) and L-glutamine. Separately derived primary cultures of dermal fibroblasts from newborn matching wt, syndecan-1 null, s4ko, and double null mice were also prepared. The same medium with 5% FCS was used to grow rat embryonic fibroblasts. HaCaT cells were cultured in Ca^{2+}-free DMEM supplemented with 2 mM Glutamine and 5% dialyzed, sterile-filtered FCS. Undifferentiated HaCaT cultures were maintained in the medium supplemented with 0.03 mM Ca^{2+}, whereas differentiating cultures were maintained in 1.2 mM Ca^{2+}. All cell cultures were routinely screened for mycoplasma. Cells were transiently transfected using Lipofectamine transfection and Plus reagent (Invitrogen) according to the manufacturer's instructions. Transgene expression was analyzed 24–48 h after transfection. Plasmids for transfections were isolated from transformed bacteria expressing specific plasmids using High Pure Plasmid Isolation kit (Roche) according to the manufacturer's instructions. wt syndecan-4 (*wtSDC4*), truncated syndecan-4 (*SDC4-Δ191I*), heparan sulfate–deficient syndecan-4 (*SDC4-AAA*), and pQE-30-HepII plasmids were produced as described previously (Gopal et al., 2010). In brief, full-length rat syndecan-4 cDNA was inserted into pIRES2-EGFP (expression vector under the CMV promoter; Takara Bio Inc.) using primers complementary to the 5′ and 3′ noncoding regions of syndecan-4 and containing EcoRI and BamHI restriction sites. The heparan sulfate–deficient syndecan-4 (*SDC4-AAA*) mutant was generated by mutating the three serine residues (44, 65, and 67), which serve as syndecan-4 glycosaminoglycan attachment sites, to alanine residues. The truncated syndecan-4 (*SDC4-Δ191I*) was generated from the full-length rat syndecan-4 by truncating the variable region in cytoplasm domain after residue 191, using a specific primer containing a BamHI

restriction site. Recombinant His-tagged HepII ($FNIII_{12–15}$) domain was prepared by polymerase chain reaction by using human cDNA as a template and primers to the 5′ end of $FNIII_{12}$ and the 3′ end of $FNIII_{15}$. The product was inserted into the bacterial expression vector pQE-30 with the T5 promoter (QIAGEN). Phospho-mimetic (*TRPC7-S714E*) and phospho-resistant (*TRPC7-S714A*) forms of TRPC7 were produced by introducing point mutations in wt TRPC7 (*wtTRPC7*) plasmid using the primers S714E AGT→GCT (forward primer, 5′-CCTGCTCCTTTTAATCTAGTGCCAGCTCCTAATCATTTTATTATCTC-3′; reverse primer, 5′-GAGATAATAAAATGATTAGGAGCTGGCACTAGATTAAAAGGAGCAGG-3′) and S714A AGT→GAA (forward primer, 5′-CCTGCTCCTTTTAATCTAGTGCCAGAACCTAATCATTTTATTATCTC-3′; reverse primer, 5′-GAGATAATAAAATGATTAGGTTCTGGCACTAGATTAAAAGGAGCAGG-3′).

Troponin C–based ratiometric calcium sensing FRET probe Twitch-1 in pcDNA3 plasmid was reported previously (Thestrup et al., 2014). In brief, cDNA of toadfish Troponin C derived from swim bladder was used to design a minimal domain calcium indicator. The general structure of the calcium biosensor is as follows: ECFP/Cer3/mTurquoise2-Sphl-linker-minimal calcium binding-linker-SacI-Met cpCitrine174/cpVenus^{CD}-Stop. The Twitch-1 sensor was inserted into the CMV promoter containing plasmid pcDNA3 using specific primers containing restriction sites for BamHI and NotI.

C. elegans mutant and transgenic reporter strains

Strains were grown using standard growth conditions on nematode growth media agar at 20°C on *Escherichia coli* OP50 (Brenner, 1974). Mutant alleles used (backcrossed five times to N2 before analysis) were *sdn-1(zh20)*, *trp-1(ok323)*, and *trp-2(gk298)*. Transgenic reporter strains used were *oyIs14* (PVQ::gfp marker), *zdIs13* (HSN::gfp marker), and wzls115 *rab-3^{prom}::camelonYC3.60* (Pedersen et al., 2013; Smith et al., 2013).

Mouse and rat strains

TRPC4 null and matching wt rats have been described previously (Alzoubi et al., 2013). In brief, *TRPC4* KO Fisher 344 rats were generated by Transposagen Biopharmaceuticals as part of the Knockout Rat Consortium and were bred and genotyped as described previously (Alzoubi et al., 2013). Matching wt Fisher 344 rats were used as controls. Genomic DNA was subjected to PCR and generated a 905-bp product in controls and 510-bp product in null rats (Alzoubi et al., 2013). wt littermates and Sdc1$^{-/-}$ and Sdc4$^{-/-}$ single KO mice, and Sdc1$^{-/-}$ and Sdc4$^{-/-}$ double KO mice on the C57BL/6J background were used at an age of 6–8 d. Using a IRESβGeo cassette with appropriate 5′ and 3′ regions of the syndecan-4 genomic DNA, deletion of exons 2–4 of syndecan-4 core protein DNA was achieved, as described previously (Echtermeyer et al., 2001). PCR analysis confirmed a 2,900-bp product from wt genomic DNA and 2,300-bp product from s4ko genomic DNA. Mutational insertion of a PGKneo cassette in the signal sequence of syndecan-1 exon 1 was achieved as described previously (Alexander et al., 2000). PCR of genomic DNA confirmed a 231-bp product from wt and a 450-bp product from null mice. The Sdc1$^{-/-}$/Sdc4$^{-/-}$ double KO mice were generated by mating Sdc1$^{-/-}$ and Sdc4$^{-/-}$ mice backcrossed at least 10 times onto the C57BL/6J background. Then the double heterozygotes were mated and double homozygotes were identified by genotyping. When sufficient homozygotes were generated, they were interbred to each other to build the double KO colony. Therefore, the double KOs are congenic on the C57BL/6J background. Unchallenged Sdc1$^{-/-}$, Sdc4$^{-/-}$, and Sdc1$^{-/-}$/Sdc4$^{-/-}$ double KO mice are viable and fertile with normal anatomical morphology, blood cell counts, and blood chemistry. Genomic analysis of null and wt rodents is shown in Fig. S5.

Antibodies and reagents

Monoclonal antibodies used in this study included rabbit anti-αSMA antibody (clone E184; Abcam), mouse anti–α-actinin (clone BM75.2; Sigma-Aldrich), mouse anti-HA.11 (clone 16B12; Covance), mouse anti–β-tubulin (clone TUB 2.1; Sigma-Aldrich), mouse anti-paxillin (clone 5H11; EMD Millipore), mouse anti–syndecan-1 (clone B-A38; Abcam), rat anti–syndecan-4 (clone KY/8.2; BD), mouse anti-p120 catenin (clone 6H11; Invitrogen), rat anti–E-cadherin (clone DEC MA-1; Abcam), and rabbit anti-NFAT3 (clone 23E6; Cell Signaling Technology). Polyclonal antibodies used were rabbit antibodies against syndecan-4 (Abcam and LSBio), OB-cadherin (Cell Signaling Technology), N-cadherin (Abcam), P-cadherin (Cell Signaling Technology), keratin-10 (Covance), TRPC4 (Sigma-Aldrich), and TRPC7 (Sigma-Aldrich and EMD Millipore). Secondary antibodies included goat anti–rabbit, goat anti–mouse, and rabbit anti–rat IgG HRP-conjugated antibodies from Dako. Donkey and goat anti–mouse, goat anti–rabbit, and donkey and goat anti–rat IgG conjugated to Alexa Fluor 488, 568, or 647 were obtained from Molecular Probes. DAPI and Alexa Fluor 568– and 647–conjugated phalloidin were obtained from Molecular Probes.

Immunochemistry and Western blots

Immunostaining of cells was performed as described previously (Gopal et al., 2010; Okina et al., 2012). Stained samples were analyzed on a AXIOplan-2 microscope (Carl Zeiss) equipped with a CoolSNAP cf2 charge coupled device camera (Roper Scientific) using a Plan Neofluor 40×/0.7 or an apochromat 63×/1.4 oil objective. Images were acquired using Metamorph 6.2r6 (Molecular Devices). Confocal images were acquired using an inverted LSM-510 META confocal microscope (Carl Zeiss) equipped with a diode laser (405 nm), an argon laser (488 nm), and two helium-neon lasers (543 and 633 nm) and the Zen 2009 software. The 63x/1.4 oil-immersion Plan Apochromat objective (Carl Zeiss) was used with the following beamsplitters: HF405/488/543/633, NFT 545 and BP505-545, BP560-615, and LP650. Images were acquired as 16-bit TIFF files and the brightness/contrast of images was adjusted in Photoshop CS6 (Adobe). To analyze specific classes of conventional calcium channels and cellular response to calcium, mouse embryonic fibroblasts (MEFs) were treated with different calcium channel inhibitors including 10 µM Pimozide (Sigma-Aldrich; T-type channel blocker) and 10 µM Nifedipine (L-type channel inhibitor affecting some of the T-type channels) for 1 h before staining for adhesion-related proteins. Controls were performed with DMSO only in αMEM. Immunohistochemistry on skin sections from wt, syndecan null mice, and wt or TRPC4 null rats was performed as described previously (Lendorf et al., 2011). Staining was developed using the Envision detection system (Dako), followed by counterstaining with hematoxylin. Stained sections were scanned at 40× using the NanoZoomer 2.0-HT digital slide scanner (Hamamatsu Photonics). To compare expression of adhesion-related proteins and TRPC channels, cell lysates were separated on SDS-PAGE gels followed by blotting to polyvinylidene fluoride membranes. Proteins were detected using primary antibodies and appropriate HRP-conjugated secondary antibodies with the aid of a chemiluminescence kit (Biological Industries).

C. elegans microscopy

For phenotypic analysis of neuronal development, animals were anaesthetized on 5% agarose pads containing 20 mM NaN_3. Images were taken using an automated fluorescence microscope (AXIO Imager M2; Carl Zeiss) and Zen 2012 software, equipped with objectives (EC Plan-NeoFluor 20x/0.5 and 40x/0.75 and Plan Apochromat 63x/1.4 oil DIC and 100x/1.4 oil DIC; Carl Zeiss) and an ORCA-R^2 camera (C10600; Hamamatsu Photonics). For in vivo calcium imaging, *C. elegans* in L4 stage expressing the Ca^{2+} sensor Cameleon YC3.60 were immobilized with 0.10 µM polystyrene microspheres (Polybead; Polysciences Inc.) on a

glass slide coated with a 10% agarose pad. The rab-3::cameleonYC3.60 strain was obtained from N. Ringstad (New York University Langone Medical Center, New York, NY).Temperature was maintained at 25°C during which two ventral motor neurons, most anteriorly and posteriorly to the vulva, were imaged. Calcium imaging was performed as described in the In vitro calcium imaging section. Post-acquisition analysis was performed using Volocity 3D analysis software 6.3 (PerkinElmer).

C. elegans phenotypic and exploratory behavior analysis

Neuronal phenotypes were analyzed in 1-d-old adults using *gfp* reporter strains that mark PVQ (*oyIs14*) and HSN (*zdIs13*) neurons. The position of neuronal cell bodies and direction of axonal outgrowth were compared with control animals. All phenotypic scoring was performed in triplicate, on a minimum of two independent days. Neuronal phenotypes were scored in >50 animals on each occasion. For exploratory behavior, single L4 animals were placed on 35-mm plates uniformly coated with the *E. coli* OP50 strain and allowed to explore their environment for 16 h before being removed. The plates were then superimposed on a grid containing squares and the number of squares entered by the worm, by observing worm tracks, was counted manually.

In vitro calcium imaging

For live cell imaging, cells were cultured on µ-slides (Ibidi). FRET was used to analyze cytosolic calcium levels during steady-state or after transfection or chemical treatments. Before imaging, the culture medium was replaced by Leibovitz's L-15 medium without phenol red (Life Technologies) supplemented with 10% FCS. Cells expressing the calcium-sensing FRET probe Twitch-1 in pcDNA3 were imaged for donor and acceptor emissions using a DeltaVision platform (GE Healthcare) comprising a motorized, inverted microscope (IX71; Olympus; Universal Apochromat/340 40×/1.35 oil and Plan Apochromat N 60×/1.42 oil objectives with optical filters 438/24 for CFP and 513/17 for YFP excitation, 470/24 for CFP and 559/38 for YFP emission, CFP/YFP/mCherry Polychroic mirror [InsightSSI filters], LED illumination source [Lumencor], and CoolSNAP HQ2 [−25°C air cool, 8.98 × 6.71-mm imaging area 6.45 × 6.45-µm pixel size] camera [Photometrics]). All live imaging was performed at 37°C and 85% humidity. Image acquisition and post-acquisition analysis was performed using Softworx suit 2.0 and Volocity 3D analysis software 6.3 (PerkinElmer). Normalized FRET index was calculated using two different methods. For primary cell lines, Volocity software based on a published algorithm (Xia and Liu, 2001) for FRET analysis was used; background correction and threshold setting were done according to the instructions in the Volocity 3D analysis software. No brightness/contrast adjustments were applied to these images. For HaCat cells, ratiometric analysis was performed by calculating the ratio between intensity of FRET channel and the donor channel. In both cases, measurements were based on unimolecular FRET, which obviated donor–acceptor stoichiometry correction. For analyzing roles of heparan sulfate chains in calcium regulation, rat embryo fibroblasts expressing Twitch-1 were plated on fibronectin or $FnIII_{6–10}$–coated substrates for 2 h. $FnIII_{6–10}$ was provided by M. Humphries (University of Manchester, Manchester, UK). $FnIII_{12–15}$ (5 µg/well) was added to cells plated on $FnIII_{6–10}$ followed by filming for another 2 h. At the end of the experiments, calcium was depleted by EGTA and then increased by 2 µM ionomycin calcium salt (Cell Signaling Technology) in the presence of 10 mM calcium chloride to assess minimum and maximum FRET level, respectively. To investigate the role of PKCα in regulating TRPC7, wt MEFs expressing *Twitch-1* were silenced for TRPC7 expression, followed by the addition of GF109203x (1 µM). Cells were filmed for donor and acceptor emission throughout the addition of GF109203x. A similar experiment was performed with cells plated on FN or $FnIII_{6–10}$ followed by addition of $FnIII_{12–15}$. To further study this, *wtTRPC7*, *TRPC7-S714A*, and *TRPC7-S714E* were expressed in rat embryo fibroblasts followed by calcium imaging.

Syndecan–TRPC interaction

Anti–syndecan-4 antibody or equivalent IgGs were covalently coated on magnetic beads (Estapore; EMD) according to the manufacturer's instructions. In brief, 20 µl of beads from stock were washed with 500 µl of coating buffer (0.1 M sodium borate buffer, pH 9.5) two to three times, and then 30 µg of antibody or IgG and 166 µl of 3 M ammonium sulfate solution were added directly to 280 µl of coating buffer followed by incubation at room temperature. After 16 h, beads were collected and incubated in blocking solution (PBS, pH 7.4, with 1% [wt/vol] BSA and 0.1% Tween 20) for 1 h followed by rinsing with wash buffer (PBS, pH 7.4, with 0.1% [wt/vol] BSA and 0.1% Tween 20). Finally, beads were collected, resuspended in serum-free media, and applied directly on to the cells in serum-free conditions. After 1-h incubation, cells were washed with TBS to remove unbound beads, followed by cell lysis using buffer containing 50 mM Tris, pH 7.4, 150 mM NaCl, 1% Triton X-100, complete protease inhibitor (Roche), and pepstatin. The beads were collected using a magnet (Miltenyi Biotec) and washed several times using a buffer containing 50 mM Tris, pH 7.4, 150 mM NaCl, 0.1% Triton X-100, complete protease inhibitor, and pepstatin. After final wash, beads were treated with 2.5× standard Laemmli buffer followed by SDS-PAGE and Western blot using the lysate.

Electron microscopy

Transmission electron microscopy was used to study the keratinocyte organization in the skin. Mouse (wt and SDC1/4 double KO) and rat (wt and TRPC4 KO) skin samples were fixed in 2.5% glutaraldehyde in 0.05 M sodium cacodylate buffer, pH 7.4, and the specimens were routinely processed and embedded in epoxy resin. Ultra-thin sections were analyzed on a CM100 (Fei) equipped with a Veleta camera (Olympus) with a resolution of 2048 × 2048 pixels. Images were recorded and processed using the iTEM software (Fei). Frames were captured at a magnification of 7,400 and the number of cells per unit length in contact with the basement membrane (dermal–epidermal junction) were quantified using Volocity 6.3 (PerkinElmer) software.

Silencing gene expression and gene expression analysis

Silencing of genes was achieved by using smart pool siRNAs against respective genes using HiPerfect transfection reagent (QIAGEN) as per the manufacturer's instructions. Efficiency of knock down was analyzed by Western blot or quantitative RT-PCR. In brief, isolated RNA was reverse transcribed into cDNA from >400 ng of RNA using TaqMan Reverse Transcription kit (Applied Biosystems) according to the manufacturer's instructions. Quantitative PCR was performed using Fermentas Maxima SYBR green master mix (Thermo Fisher Scientific) in LightCycler480 (Roche) with 40 amplification cycles. The threshold cycle values were determined by absolute quantification analysis using the fit points method in the LightCycler software and final values were normalized against values for housekeeping genes RPO or GAPDH.

Affymetrix microarray

The Affymetrix microarray comparing gene transcription of matching wt and s4ko MEFs was described previously (Okina et al., 2012). RNA was isolated from wt and s4ko MEFs in triplicate using TRIzol (Invitrogen) as described by the manufacturer. Gene expression was compared using Affimetrix GeneChip mouse 430 2.0 platform (Microarray Center, University of Copenhagen). The microarray CEL files were read into the R statistical software (Ihaka and Gentleman, 1996) and probe set levels were calculated using the RMA algorithm with default

settings (i.e., "RMA" background correction, "quantiles" normalization, "pmonly" Perfect Match correction, and "medianpolish" probe set summary calculation).

Statistical analysis

Data are given as means ± SEM. For statistical analysis, unpaired *t* test was used. Final value and error bars were calculated from at least three different experiments. For *C. elegans* phenotypic analysis and exploratory behavior studies, one-way analysis of variance (ANOVA) was used for comparisons followed by Newman-Keuls multiple comparison test. For calcium measurements in *C. elegans*, Ca^{2+} levels were measured in 40 neurons per strain per experiment before taking means from multiple experiments. All graphs were plotted and statistical analysis was performed using GraphPad Prism 6 (GraphPad Software) or R statistical software (Foundation for Statistical Computing).

Online supplemental material

Fig. S1 shows alterations in NFATc4 and calcineurin in wt compared with s4ko fibroblasts. Also shown are controls for the calcium imaging and the mRNA expression of ion channels in the two fibroblast types. Fig. S2 shows the lack of impact of L-type and T-type calcium channel inhibitors on the actin cytoskeleton as well as the effects of depleting several TRP channels by siRNA. Also shown are expression levels of OB- and N-cadherin in wt and s4ko fibroblasts and the impact of re-expression of mutant forms of syndecan-4 in null cells. Fig. S3 shows the impact of reduction or elimination of syndecan-1 in s4ko and wt fibroblasts, in terms of cytoskeleton, junction formation, and calcium levels. Fig. S4 shows the impact of syndecan-1 and/or -4 depletion on expression of other syndecans and P-cadherin in HaCaT epidermal cells. Also shown is the expression of P-cadherin and keratin 10 in epidermis from newborn s1ko and s4ko mice. Also shown are electron micrographs of epidermal basal layers of wt mouse and rat as well as S1/S4 double KO mice and TRPC4 null rat. Fig. S5 shows genotyping of wt and KO mice and rats. Video 1 shows calcium fluctuations in wt fibroblasts expressing the Twitch-1 ratiometric sensor. Video 2 shows calcium imaging in s4ko fibroblasts expressing the Twitch-1 sensor. Video 3 shows minimum and maximum FRET levels from Twitch-1 ratiometric calcium sensor in response to EGTA followed by calcium in the presence of ionomycin. Video 4 shows the decreasing calcium levels in wt cells seeded on the central integrin-binding domain of fibronectin ($FnIII_{6–10}$) in response to addition of fibronectin HepII domain ($FnIII_{12–15}$). Calcium levels are measured in cells expressing the Twitch-1 ratiometric calcium sensor. Online supplemental material is available at http://www.jcb.org/cgi/content/full/jcb.201501060/DC1.

Acknowledgments

The authors thank Prof. Martin Humphries and Dr. Niels Ringstad for providing reagents. We thank Eva Tulin Kristensen for technical assistance and Dr. Betina Séverine Fogh for Fig. 2 C. We acknowledge the Core Facility for Integrated Microscopy, Faculty of Health and Medical Sciences, and the Microarray Center, University of Copenhagen.

This work was supported by The Danish National Research Foundation and Danish Council of Natural Sciences (J.R. Couchman), Novo Nordisk Foundation (J.R. Couchman and R. Pocock), Lundbeck Foundation (J.R. Couchman, R. Pocock, and M.E. Pedersen), European Research Council (starting grant number 260807; R. Pocock), and National Institutes of Health grants R01 HL66299 and HL60024 (T. Stevens) and R01 EY21765 (P.W. Park).

The authors declare no competing financial interests.

S. Gopal, P. Søgaard, C. Pataki, E. Okina, and X. Xian performed experimental work and analyzed data. M.E. Pedersen and R. Pocock provided materials, reagents, expertise, and contributed to the experimental work on *C. elegans*. T. Stevens and P.W. Park produced and characterized the rodents and provided tissues. H.A.B. Multhaupt carried out immunohistochemistry and electron microscopy, analyzed data, and assisted S. Gopal in manuscript preparation. J.R. Couchman was responsible for project inception, oversight, data analysis, and manuscript preparation. R. Pocock contributed to manuscript editing.

Submitted: 15 January 2015
Accepted: 25 August 2015

References

Alexander, C.M., F. Reichsman, M.T. Hinkes, J. Lincecum, K.A. Becker, S. Cumberledge, and M. Bernfield. 2000. Syndecan-1 is required for Wnt-1-induced mammary tumorigenesis in mice. *Nat. Genet.* 25:329–332. http://dx.doi.org/10.1038/77108

Alzoubi, A., P. Almalouf, M. Toba, K. O'Neill, X. Qian, M. Francis, M.S. Taylor, M. Alexeyev, I.F. McMurtry, M. Oka, and T. Stevens. 2013. TRPC4 inactivation confers a survival benefit in severe pulmonary arterial hypertension. *Am. J. Pathol.* 183:1779–1788. http://dx.doi.org/10.1016/j.ajpath.2013.08.016

Amaral, M.D., and L. Pozzo-Miller. 2007. TRPC3 channels are necessary for brain-derived neurotrophic factor to activate a nonselective cationic current and to induce dendritic spine formation. *J. Neurosci.* 27:5179–5189. http://dx.doi.org/10.1523/JNEUROSCI.5499-06.2007

Ambudkar, I.S., B.C. Bandyopadhyay, X. Liu, T.P. Lockwich, B. Paria, and H.L. Ong. 2006. Functional organization of TRPC-Ca^{2+} channels and regulation of calcium microdomains. *Cell Calcium.* 40:495–504. http://dx.doi.org/10.1016/j.ceca.2006.08.011

Baietti, M.F., Z. Zhang, E. Mortier, A. Melchior, G. Degeest, A. Geeraerts, Y. Ivarsson, F. Depoortere, C. Coomans, E. Vermeiren, et al. 2012. Syndecan–syntenin–ALIX regulates the biogenesis of exosomes. *Nat. Cell Biol.* 14:677–685. http://dx.doi.org/10.1038/ncb2502

Barbouri, D., N. Afratis, C. Gialeli, D.H. Vynios, A.D. Theocharis, and N.K. Karamanos. 2014. Syndecans as modulators and potential pharmacological targets in cancer progression. *Front. Oncol.* 4:4. http://dx.doi.org/10.3389/fonc.2014.00004

Bass, M.D., R.C. Williamson, R.D. Nunan, J.D. Humphries, A. Byron, M.R. Morgan, P. Martin, and M.J. Humphries. 2011. A syndecan-4 hair trigger initiates wound healing through caveolin- and RhoG-regulated integrin endocytosis. *Dev. Cell.* 21:681–693. http://dx.doi.org/10.1016/j.devcel.2011.08.007

Beck, B., V. Lehen'kyi, M. Roudbaraki, M. Flourakis, M. Charveron, P. Bordat, R. Polakowska, N. Prevarskaya, and R. Skryma. 2008. TRPC channels determine human keratinocyte differentiation: new insight into basal cell carcinoma. *Cell Calcium.* 43:492–505. http://dx.doi.org/10.1016/j.ceca.2007.08.005

Bishop, J.R., M. Schuksz, and J.D. Esko. 2007. Heparan sulphate proteoglycans fine-tune mammalian physiology. *Nature.* 446:1030–1037. http://dx.doi.org/10.1038/nature05817

Brenner, S. 1974. The genetics of *Caenorhabditis elegans*. *Genetics.* 77:71–94.

Bülow, H.E., and O. Hobert. 2004. Differential sulfations and epimerization define heparan sulfate specificity in nervous system development. *Neuron.* 41:723–736. http://dx.doi.org/10.1016/S0896-6273(04)00084-4

Chen, K., and K.J. Williams. 2013. Molecular mediators for raft-dependent endocytosis of syndecan-1, a highly conserved, multifunctional receptor. *J. Biol. Chem.* 288:13988–13999. http://dx.doi.org/10.1074/jbc.M112.444737

Couchman, J.R. 2010. Transmembrane signaling proteoglycans. *Annu. Rev. Cell Dev. Biol.* 26:89–114. http://dx.doi.org/10.1146/annurev-cellbio-100109-104126

Davis, J., A.R. Burr, G.F. Davis, L. Birnbaumer, and J.D. Molkentin. 2012. A TRPC6-dependent pathway for myofibroblast transdifferentiation and wound healing in vivo. *Dev. Cell.* 23:705–715. http://dx.doi.org/10.1016/j.devcel.2012.08.017

Dovas, A., A. Yoneda, and J.R. Couchman. 2006. PKCβ-dependent activation of RhoA by syndecan-4 during focal adhesion formation. *J. Cell Sci.* 119:2837–2846. http://dx.doi.org/10.1242/jcs.03020

Echtermeyer, F., M. Streit, S. Wilcox-Adelman, S. Saoncella, F. Denhez, M. Detmar, and P. Goetinck. 2001. Delayed wound repair and impaired

angiogenesis in mice lacking syndecan-4. *J. Clin. Invest.* 107:R9–R14. http://dx.doi.org/10.1172/JCI10559

Echtermeyer, F., T. Harendza, S. Hubrich, A. Lorenz, C. Herzog, M. Mueller, M. Schmitz, A. Grund, J. Larmann, J. Stypmann, et al. 2011. Syndecan-4 signalling inhibits apoptosis and controls NFAT activity during myocardial damage and remodelling. *Cardiovasc. Res.* 92:123–131. http://dx.doi.org/10.1093/cvr/cvr149

Ethell, I.M., F. Irie, M.S. Kalo, J.R. Couchman, E.B. Pasquale, and Y. Yamaguchi. 2001. EphB/syndecan-2 signaling in dendritic spine morphogenesis. *Neuron.* 31:1001–1013. http://dx.doi.org/10.1016/S0896-6273(01)00440-8

Fabian, A., T. Fortmann, E. Bulk, V.C. Bomben, H. Sontheimer, and A. Schwab. 2011. Chemotaxis of MDCK-F cells toward fibroblast growth factor-2 depends on transient receptor potential canonical channel 1. *Pflugers Arch.* 461:295–306. http://dx.doi.org/10.1007/s00424-010-0901-6

Finsen, A.V., I.G. Lunde, I. Sjaastad, E.K. Østli, M. Lyngra, H.O. Jarstadmarken, A. Hasic, S. Nygård, S.A. Wilcox-Adelman, P.F. Goetinck, et al. 2011. Syndecan-4 is essential for development of concentric myocardial hypertrophy via stretch-induced activation of the calcineurin-NFAT pathway. *PLoS ONE.* 6:e28302. http://dx.doi.org/10.1371/journal.pone.0028302

Giannone, G., P. Rondé, M. Gaire, J. Beaudouin, J. Haiech, J. Ellenberg, and K. Takeda. 2004. Calcium rises locally trigger focal adhesion disassembly and enhance residency of focal adhesion kinase at focal adhesions. *J. Biol. Chem.* 279:28715–28723. http://dx.doi.org/10.1074/jbc.M404054200

Goel, M., W. Sinkins, A. Keightley, M. Kinter, and W.P. Schilling. 2005. Proteomic analysis of TRPC5- and TRPC6-binding partners reveals interaction with the plasmalemmal Na^+/K^+-ATPase. *Pflugers Arch.* 451:87–98. http://dx.doi.org/10.1007/s00424-005-1454-y

Gopal, S., A. Bober, J.R. Whiteford, H.A. Multhaupt, A. Yoneda, and J.R. Couchman. 2010. Heparan sulfate chain valency controls syndecan-4 function in cell adhesion. *J. Biol. Chem.* 285:14247–14258. http://dx.doi.org/10.1074/jbc.M109.056945

Greene, D.K., S. Tumova, J.R. Couchman, and A. Woods. 2003. Syndecan-4 associates with α-actinin. *J. Biol. Chem.* 278:7617–7623. http://dx.doi.org/10.1074/jbc.M207123200

Hakuno, M., M. Akiyama, H. Shimizu, M.J. Wheelock, and T. Nishikawa. 2001. Upregulation of P-cadherin expression in the lesional skin of pemphigus, Hailey-Hailey disease and Darier's disease. *J. Cutan. Pathol.* 28:277–281. http://dx.doi.org/10.1034/j.1600-0560.2001.028006277.x

Hayakawa, K., H. Tatsumi, and M. Sokabe. 2008. Actin stress fibers transmit and focus force to activate mechanosensitive channels. *J. Cell Sci.* 121:496–503. http://dx.doi.org/10.1242/jcs.022053

Hinz, B., P. Pittet, J. Smith-Clerc, C. Chaponnier, and J.J. Meister. 2004. Myofibroblast development is characterized by specific cell-cell adherens junctions. *Mol. Biol. Cell.* 15:4310–4320. http://dx.doi.org/10.1091/mbc.E04-05-0386

Horowitz, A., and M. Simons. 1998. Phosphorylation of the cytoplasmic tail of syndecan-4 regulates activation of protein kinase Cα. *J. Biol. Chem.* 273:25548–25551. http://dx.doi.org/10.1074/jbc.273.40.25548

Ihaka, R., and R. Gentleman. 1996. A language for data analysis and graphics. *J. Comput. Graph. Stat.* 5:299–314.

Kinnunen, T., M. Kaksonen, J. Saarinen, N. Kalkkinen, H.B. Peng, and H. Rauvala. 1998. Cortactin-Src kinase signaling pathway is involved in N-syndecan-dependent neurite outgrowth. *J. Biol. Chem.* 273:10702–10708. http://dx.doi.org/10.1074/jbc.273.17.10702

Kinnunen, T., Z. Huang, J. Townsend, M.M. Gatdula, J.R. Brown, J.D. Esko, and J.E. Turnbull. 2005. Heparan 2-*O*-sulfotransferase, *hst-2*, is essential for normal cell migration in *Caenorhabditis elegans*. *Proc. Natl. Acad. Sci. USA.* 102:1507–1512. http://dx.doi.org/10.1073/pnas.0401591102

Langford, P.R., L. Keyes, and M.D. Hansen. 2012. Plasma membrane ion fluxes and NFAT-dependent gene transcription contribute to c-met-induced epithelial scattering. *J. Cell Sci.* 125:4001–4013. http://dx.doi.org/10.1242/jcs.098269

Lendorf, M.E., T. Manon-Jensen, P. Kronqvist, H.A. Multhaupt, and J.R. Couchman. 2011. Syndecan-1 and syndecan-4 are independent indicators in breast carcinoma. *J. Histochem. Cytochem.* 59:615–629. http://dx.doi.org/10.1369/0022155411405057

Leuner, K., M. Kraus, U. Woelfle, H. Beschmann, C. Harteneck, W.H. Boehncke, C.M. Schempp, and W.E. Müller. 2011. Reduced TRPC channel expression in psoriatic keratinocytes is associated with impaired differentiation and enhanced proliferation. *PLoS ONE.* 6:e14716. http://dx.doi.org/10.1371/journal.pone.0014716

Li, Q., P.W. Park, C.L. Wilson, and W.C. Parks. 2002. Matrilysin shedding of syndecan-1 regulates chemokine mobilization and transepithelial efflux of neutrophils in acute lung injury. *Cell.* 111:635–646. http://dx.doi.org/10.1016/S0092-8674(02)01079-6

Martínez-Martínez, S., L. Genescà, A. Rodríguez, A. Raya, E. Salichs, F. Were, M.D. López-Maderuelo, J.M. Redondo, and S. de la Luna. 2009. The RCAN carboxyl end mediates calcineurin docking-dependent inhibition via a site that dictates binding to substrates and regulators. *Proc. Natl. Acad. Sci. USA.* 106:6117–6122. http://dx.doi.org/10.1073/pnas.0812544106

Morgan, M.R., M.J. Humphries, and M.D. Bass. 2007. Synergistic control of cell adhesion by integrins and syndecans. *Nat. Rev. Mol. Cell Biol.* 8:957–969. http://dx.doi.org/10.1038/nrm2289

Morgan, M.R., H. Hamidi, M.D. Bass, S. Warwood, C. Ballestrem, and M.J. Humphries. 2013. Syndecan-4 phosphorylation is a control point for integrin recycling. *Dev. Cell.* 24:472–485. http://dx.doi.org/10.1016/j.devcel.2013.01.027

Mostafavi-Pour, Z., J.A. Askari, S.J. Parkinson, P.J. Parker, T.T.C. Ng, and M.J. Humphries. 2003. Integrin-specific signaling pathways controlling focal adhesion formation and cell migration. *J. Cell Biol.* 161:155–167. http://dx.doi.org/10.1083/jcb.200210176

Oh, E.S., A. Woods, and J.R. Couchman. 1997. Syndecan-4 proteoglycan regulates the distribution and activity of protein kinase C. *J. Biol. Chem.* 272:8133–8136. http://dx.doi.org/10.1074/jbc.272.13.8133

Okina, E., A. Grossi, S. Gopal, H.A. Multhaupt, and J.R. Couchman. 2012. α-actinin interactions with syndecan-4 are integral to fibroblast–matrix adhesion and regulate cytoskeletal architecture. *Int. J. Biochem. Cell Biol.* 44:2161–2174. http://dx.doi.org/10.1016/j.biocel.2012.08.017

Pani, B., E. Cornatzer, W. Cornatzer, D.M. Shin, M.R. Pittelkow, A. Hovnanian, I.S. Ambudkar, and B.B. Singh. 2006. Up-regulation of transient receptor potential canonical 1 (TRPC1) following sarco(endo)plasmic reticulum Ca^{2+} ATPase 2 gene silencing promotes cell survival: a potential role for TRPC1 in Darier's disease. *Mol. Biol. Cell.* 17:4446–4458. http://dx.doi.org/10.1091/mbc.E06-03-0251

Pap, T., and J. Bertrand. 2013. Syndecans in cartilage breakdown and synovial inflammation. *Nat. Rev. Rheumatol.* 9:43–55. http://dx.doi.org/10.1038/nrrheum.2012.178

Pedersen, M.E., G. Snieckute, K. Kagias, C. Nehammer, H.A. Multhaupt, J.R. Couchman, and R. Pocock. 2013. An epidermal microRNA regulates neuronal migration through control of the cellular glycosylation state. *Science.* 341:1404–1408. http://dx.doi.org/10.1126/science.1242528

Prager-Khoutorsky, M., A. Lichtenstein, R. Krishnan, K. Rajendran, A. Mayo, Z. Kam, B. Geiger, and A.D. Bershadsky. 2011. Fibroblast polarization is a matrix-rigidity-dependent process controlled by focal adhesion mechanosensing. *Nat. Cell Biol.* 13:1457–1465. http://dx.doi.org/10.1038/ncb2370

Ramani, V.C., A. Purushothaman, M.D. Stewart, C.A. Thompson, I. Vlodavsky, J.L. Au, and R.D. Sanderson. 2013. The heparanase/syndecan-1 axis in cancer: mechanisms and therapies. *FEBS J.* 280:2294–2306. http://dx.doi.org/10.1111/febs.12168

Rhiner, C., S. Gysi, E. Fröhli, M.O. Hengartner, and A. Hajnal. 2005. Syndecan regulates cell migration and axon guidance in *C. elegans*. *Development.* 132:4621–4633. http://dx.doi.org/10.1242/dev.02042

Rybinski, B., J. Franco-Barraza, and E. Cukierman. 2014. The wound healing, chronic fibrosis, and cancer progression triad. *Physiol. Genomics.* 46:223–244. http://dx.doi.org/10.1152/physiolgenomics.00158.2013

Schwabiuk, M., L. Coudiere, and D.C. Merz. 2009. SDN-1/syndecan regulates growth factor signaling in distal tip cell migrations in *C. elegans*. *Dev. Biol.* 334:235–242. http://dx.doi.org/10.1016/j.ydbio.2009.07.020

Smith, E.S., L. Martinez-Velazquez, and N. Ringstad. 2013. A chemoreceptor that detects molecular carbon dioxide. *J. Biol. Chem.* 288:37071–37081. http://dx.doi.org/10.1074/jbc.M113.517367

Smutny, M., and A.S. Yap. 2010. Neighborly relations: cadherins and mechanotransduction. *J. Cell Biol.* 189:1075–1077. http://dx.doi.org/10.1083/jcb.201005151

Stanford, K.I., J.R. Bishop, E.M. Foley, J.C. Gonzales, I.R. Niesman, J.L. Witztum, and J.D. Esko. 2009. Syndecan-1 is the primary heparan sulfate proteoglycan mediating hepatic clearance of triglyceride-rich lipoproteins in mice. *J. Clin. Invest.* 119:3236–3245.

Stepp, M.A., H.E. Gibson, P.H. Gala, D.D. Iglesia, A. Pajoohesh-Ganji, S. Pal-Ghosh, M. Brown, C. Aquino, A.M. Schwartz, O. Goldberger, et al. 2002. Defects in keratinocyte activation during wound healing in the syndecan-1-deficient mouse. *J. Cell Sci.* 115:4517–4531. http://dx.doi.org/10.1242/jcs.00128

Tecle, E., C.A. Diaz-Balzac, and H.E. Bülow. 2013. Distinct 3-*O*-sulfated heparan sulfate modification patterns are required for *kal-1*–dependent neurite branching in a context-dependent manner in *Caenorhabditis elegans*. *G3 (Bethesda).* 3: 541–552.

Thestrup, T., J. Litzlbauer, I. Bartholomäus, M. Mues, L. Russo, H. Dana, Y. Kovalchuk, Y. Liang, G. Kalamakis, Y. Laukat, et al. 2014. Optimized ratiometric calcium sensors for functional in vivo imaging of neurons and

T lymphocytes. *Nat. Methods.* 11:175–182. http://dx.doi.org/10.1038/nmeth.2773

Trebak, M., N. Hempel, B.J. Wedel, J.T. Smyth, G.S. Bird, and J.W. Putney Jr. 2005. Negative regulation of TRPC3 channels by protein kinase C-mediated phosphorylation of serine 712. *Mol. Pharmacol.* 67:558–563. http://dx.doi.org/10.1124/mol.104.007252

Venkatachalam, K., and C. Montell. 2007. TRP channels. *Annu. Rev. Biochem.* 76:387–417. http://dx.doi.org/10.1146/annurev.biochem.75.103004.142819

Woods, A., and J.R. Couchman. 1998. Syndecans: synergistic activators of cell adhesion. *Trends Cell Biol.* 8:189–192. http://dx.doi.org/10.1016/S0962-8924(98)01244-6

Woods, A., J.R. Couchman, S. Johansson, and M. Höök. 1986. Adhesion and cytoskeletal organisation of fibroblasts in response to fibronectin fragments. *EMBO J.* 5:665–670.

Xia, Z., and Y. Liu. 2001. Reliable and global measurement of fluorescence resonance energy transfer using fluorescence microscopes. *Biophys. J.* 81:2395–2402. http://dx.doi.org/10.1016/S0006-3495(01)75886-9

Xiao, R., and X.Z. Xu. 2009. Function and regulation of TRP family channels in *C. elegans*. *Pflugers Arch.* 458:851–860. http://dx.doi.org/10.1007/s00424-009-0678-7

Zhou, S., N. Matsuyoshi, T. Takeuchi, Y. Ohtsuki, and Y. Miyachi. 2003. Reciprocal altered expression of T-cadherin and P-cadherin in psoriasis vulgaris. *Br. J. Dermatol.* 149:268–273. http://dx.doi.org/10.1046/j.1365-2133.2003.05464.x